Preprints of the 21st IFAC World Congress (Virtual)
Berlin, Germany, July 12-17, 2020

A Robotic Device for the Structural Dynamics Inspection of Railway Pantographs through Nonlinearity Tests

G. Santamato * **D. Chiaradia M. Solazzi A. Frisoli**

* *All the Authors are with Scuola Superiore Sant'Anna, Pisa 56010 ITALY (e-mail: g.santamato@santannapisa.it).*

Abstract: The railway industry is progressively embracing mechatronics solutions to improve maintenance operations. In this context, we present a robotic device that introduces structural dynamics analysis in railway pantograph inspection. Specifically, an innovative macro-micro actuation extends the bandwidth performance of actual devices, while a force control strategy proved to support the execution of nonlinearity tests via the estimation of the Frequency Response Function for different levels of the input force. Thereupon we show that the exploitation of nonlinearity can enhance the detection of even a minor localized fault.

Keywords: Structural analysis and residual evaluation methods, FDI for nonlinear Systems

1. INTRODUCTION

The emergence of high-speed railways is progressively leading to the introduction of more and more sophisticated maintenance routines, Stern (2017). In this context, strong efforts have been focused on railway pantograph, Fig. 1 (a), a special mechanism mounted on the roof of electrical trains to capture current from the high-voltage line. Its main component is the *pan head*, endowing proper contact strips and supported by a frame and an elastic suspension. When the suspension spring is actuated, an upward force is generated so as to lift the frame until the head gets in contact with the line. The critical point with the pantograph is that even localized and progressive damages in both the suspension and the frame proved to affect the energy absorption, Zhang et al. (2018), Peters (1981) as well as introduce a risk for the safety, R.A.I.B. (2013), Conway (2008).

However, pantograph maintenance still relies on periodic human inspections while structural dynamic tests are reserved for the overhaul. In the standard procedure, one point of the frame is excited by a dynamic load and both the excitation and the consequent response are simultaneously acquired. A Frequency Response Function (FRF) is generally estimated, being an efficient metric to characterize the dynamics in the frequency band of the excitation as well as a sensitive feature towards several kinds of faults, Ewins (1984); Sohn et al. (2003); Fanning et al. (2003); Fanning and Carden (2004). Currently, these indoor tests are performed by means of gantry test-rigs, equipped with heavy electro-hydraulic actuators, able to achieve an excitation bandwidth of about 100 Hz, Deml et al. (2001); Bruni et al. (2011); Xin et al. (2018). Nevertheless, industries advocate for more frequent dynamic interrogations between consecutive overhauls to further prevent failures. To this end, a number of patents, Xie et al. (2009); Bing et al. (2018); Lu (1998), disclose portable devices that can be on purpose installed on the train roof in the occasion of the periodic assessment. All of these succeed to contain weight under 20 kg by adopting a lightweight flexible actuation, but guarantee a limited bandwidth for force transmission. Consequently, low-frequency tests are allowed, averting only macroscopic faults in the suspension, with no clue about the structural integrity.

More in general, one concern with all current routines is the assumption of linearity, which fails because of the presence of not negligible friction in the frame joints. Hence the estimated FRF provides a partial description of the dynamics. Besides, damage detection itself could be enhanced if the system's nonlinearity was taken into account, Worden et al. (2008). A widely used method to deal with nonlinearity is to perform a *homogeneity test*, Worden (2019), whose aim is to ascertain if the FRFs derived from different levels of the input force overlay. In this regard, a critical aspect is that external disturbances generate distortion in the spectrum of the applied input force, Peterson (1993). Thereupon results might be misleading since one assumption of the homogeneity test is that the spectrum of the input force is constant across the whole excitation bandwidth. In this context, robotics solutions can significantly lead to in-depth and more effective maintenance.

In this paper, we present a robotic device for the *on-site* execution of dynamic tests on railway pantographs. Specifically, we conceived and experimentally validated an innovative actuation that achieves a bandwidth of 25 Hz for the transmitted force, while complying with the threshold of 20 kg typical of actual devices. Afterward, it is shown the need for a force control strategy to reject spectral disturbances on the input excitation. Subsequently, a homogeneity test was carried out to derive the pantograph FRF for 2 levels of the input force and evident nonlinear behavior was observed even in a limited frequency interval. The main contribution of this work is to show that the exploitation of nonlinearities can advantage the detection of even a minor localized fault. Indeed, the emergence of FRF alterations induced by a progressive loss of a bolted connection revealed to be dependant on the input level.

⋆ The Authors would like to thank Trenitalia SpA for the support given during the research activities.

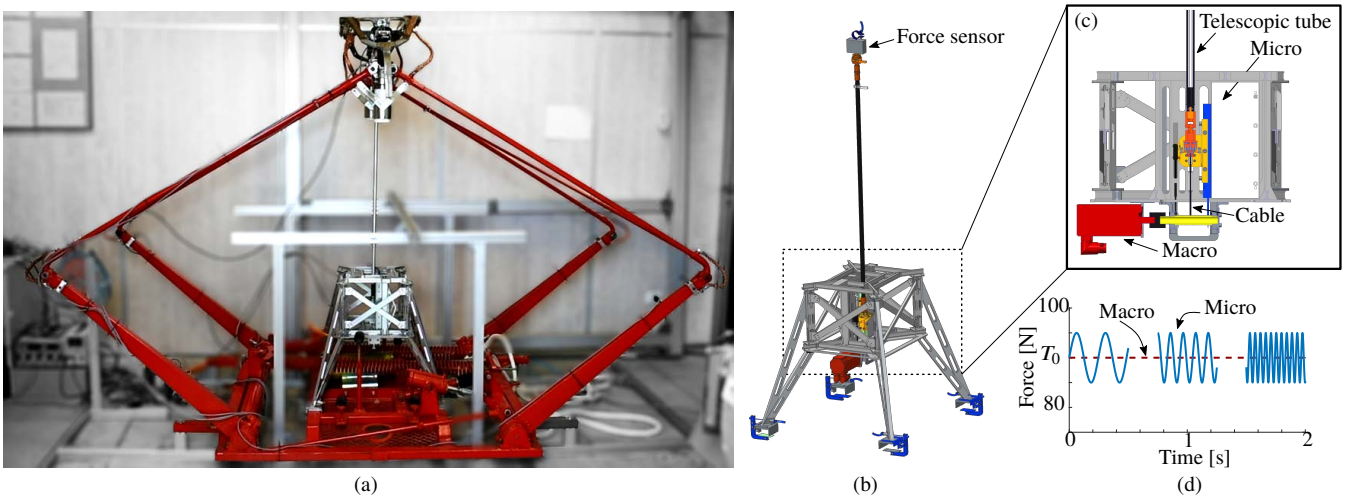

Fig. 1. (a) Railway pantograph and prototype of the inspection robot for the execution of dynamic tests. (b) Lightweight frame architecture of the robot. (c) Detail of the actuation showing the presence of a macro-micro actuation (d) Static and dynamic components of the force profile with the correspondent assignment between actuators.

2. MECHANICAL ARCHITECTURE

Fig. 1 (a) depicts the railway pantograph and a prototype of the robotic device. During the execution of the dynamic test, the pantograph is required to be set at a fixed height while a stinger-tube transmits the dynamic excitation. The working point can be adjusted since the stinger-tube is telescopic. The robot-body, pictured in Fig. 1 (b), is an aluminum-alloy skeletal frame in which a central core, hosting the actuation unit, is supported by four legs. In particular, the device can be grounded to the fixed base of the pantograph through quick-release clamping mechanisms (in dark at the bottom of each leg), so mounting operations are easy for the maintainer.

Fig. 1 (c) shows the architecture of the actuation core, which implements the principle of parallel macro-micro actuation, described in Morrell and Salisbury (1998). The need for a double actuation emerges from Fig. 1 (d) which schematizes the typical force profile necessary to excite the structure of a railway pantograph. Specifically, the excitation is composed of a main, high amplitude static contribution T_0 and a low-amplitude high-frequency dynamic signal. The presence of the static term arises from the upwards pushing force generated by the suspension which lifts the frame and pushes the pan head against the line. During the dynamic test, the pantograph must not be in contact with the catenary and hence the testing device is asked to provide the term T_0 to balance said upwards force and keep the pantograph at a fixed height. Simultaneously a dynamic force is necessary to induce the vibration regime. Therefore the need for such a constant term has the only effect to increase the range of force required to the actuation. In addition, these contributions happen to be significantly different in amplitude; while the static force settles about 90 N, an instantaneous amplitude of about 10 N is generally sufficient to excite the pantograph in the 0 - 25 Hz interval, Santamato et al. (2019).

Patents for portable devices adopt a flexible architecture in which the entire force profile is transmitted to the pantograph through a long steel cable, whose tension is regulated by a rotary motor-pulley system. Despite simplicity and lightweight, the achievable bandwidth of the excitation is unsatisfactory for structural damage detection, because of the low stiffness of the cable relative to the inertia of the motor-pulley. On the other side, commonly used shakers for dynamic tests guarantee high dynamic performances but do not generate a static force. In our implementation, the principle of motor-cable actuation is combined with an electromagnetic linear motor. In this way, it is possible to advantageously attribute each component of the excitation law to the optimal actuator. The advantageous force/weight characteristic of the motor-cable is exploited to cover the substantial portion of the excitation amplitude, meaning that a so-called *macro* actuator provides the mean force T_0 and, consequently, a *micro* electromagnetic actuator is sufficient to generate the remaining component of the excitation law. In this architecture, the steel cable couples the two motors. Hence the effective transmission of the force to the structure requires that the natural frequency of the rotary motor-cable is sufficiently above the frequency interval of the excitation, Santamato et al. (2018).

For both motor-units, a brushless direct-drive configuration has been adopted. The main advantage of this choice is the absence of mechanical transmissions that introduce friction, backlash and sensibly increase the perceived inertia. The micro-actuator is equipped with an electromagnetic linear motor whose permanent-magnets track is fixed to the robot frame while an iron-less coil is constrained to a linear guide so as to move vertically. The moving coil is provided with a mechanical interface that hosts the telescopic tube and a Hall-effect digital encoder. This sensor is necessary for the commutation of the winding phases and it is also used as sensor displacement. The end-effector is equipped with a mono-axial force sensor, fundamental to complete the *input-output* measurement and to control the actual force exerted to the structure.

3. FORCE CONTROL

3.1 Need for force control

The estimation of the Frequency Response Function (FRF) is a well-known method to visualize the input-output properties of complex systems and structures. Moreover, its computation from data records is immediate. If, for example, we denote by $f_{meas}(t)$ and $x_{meas}(t)$ the input force and the output displacement

respectively, the non-parametric estimate, McKelvey and Guérin (2012), of the so-called *receptance* FRF is:

$$FRF(\omega) = \frac{X_{meas}(\omega)}{F_{meas}(\omega)} \tag{1}$$

in which the capital letter stands for the discrete Fourier transform.

FRF contains several information regarding the dynamics of a structure, such as resonances, anti-resonances, and modal density. One further advantage in the use of FRF data for structural monitoring is that it negates the need for identification exercises. Indeed, changes in a continuously or intermittently monitored FRF can be caught by visual inspection or by simple metrics, like the mean-square error between the FRFs. Alterations in amplitude, damping, and frequencies are in particular first indicators of the occurrence of damage.

What is more, the estimation of the FRF is also a method to ascertain the nonlinearity of a system, through the so-called homogeneity test. Linearity is ensured by repeating the dynamic test several times but changing the input level over a range of values. If the FRFs derived from the different levels overlay, linearity is assumed to hold. Conversely, if the system is nonlinear, the FRF would result altered and the exact form of distortion could be related to the type of nonlinearity.

One concern with the homogeneity test arises from the fact that during the dynamic test, actuator inertia, friction in the transmission and structure/exciter interaction generate distortions and local alterations in the frequency spectrum of the applied force. In particular, when the frequency of the input force signal passes through the structural resonances, the force spectrum exhibits a strong reduction, known as *drop-off*. For nonlinear structures, this could bring to misleading estimates of the FRF. Therefore a high-performance force control is required to achieve an almost constant profile for the spectrum of the excitation.

3.2 Controller design

The control strategy was meant to drive the true applied force f_{meas} as close as possible to the desired reference law f_{ref}. In particular, since we are interested in the spectral characteristics of the force transmission, a Force Transfer Function FTF was defined in the frequency domain as follows:

$$FTF(\omega) = \frac{F_{meas}(\omega)}{F_{ref}(\omega)} \tag{2}$$

where again the capital letter stands for the Discrete Fourier Transform. A prior step to the design aimed to ascertain that no internal resonances of the passive actuation affect the force transmission in the frequency interval of the excitation. The blue-dotted curve in Fig. 2 refers to the FTF of the macro-micro actuator, in the form of a Bode plot, estimated by keeping fixed the end-effector while commanding in open-loop a linear chirp signal (with amplitude 5 N and frequency sweeping from 0.01 to 25 Hz). As expected, the force at the end-effector is affected by inertia and friction. This is reflected by an attenuation of the magnitude of the FTF that stays around a value of -5 dB. Since the magnitude and the phase lag exhibit an almost flat profile in the entire range, we can conclude that the actuator is mechanically adequate to work in this band.

Afterward, a direct force control strategy was designed, whose scheme is depicted in Fig. 3. In the control strategy, the static term T_0 equal to the pushing force is commanded to the

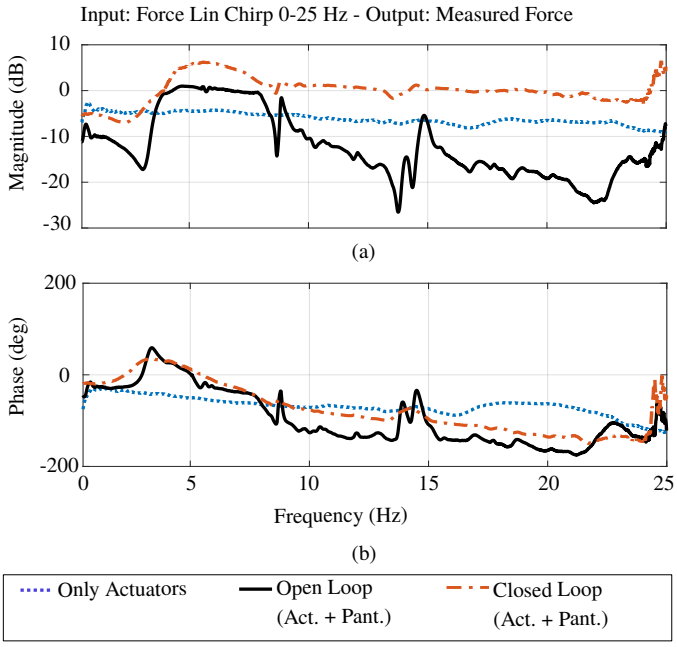

Fig. 2. Experimental estimates of the Force Transfer Function (Bode Plot)

macro actuator as a feed-forward contribution, since its value is constant and known. Such a choice is also effective for narrow-band rejection since this term is a substantial contribution in terms of the amplitude of the overall desired force law, schematized in Fig. 1 (d). Instead, the control action is demanded to the micro-actuator, since it is capable of large bandwidth performance due to its high mechanical impedance.

In a preliminary stage, since the dynamics of the overall system was not known, we experimentally estimated the FTF in open loop with the aim to compensate for the main disturbances, due to the drop-off. Practically, we defined a function $\hat{G}_{est}$ which is expressed as follows:

$$\hat{G}_{est}(\omega) = FTF(\omega)|_{openloop} \tag{3}$$

To refine the substantial action provided by the feed-forward, that is rejecting all the minor dynamic disturbances, a closed-feedback loop was designed. In particular, to achieve a better spectral match with the desired force, the tuning of a proportional gain P revealed to be sufficient. Besides, the adopted requirement for the force-tracking aimed to obtain an under-damped response with a 5% overshoot for a step input of 7.5 N. At the same time, a viscous term was added to widen the proportional gain. In Fig. 3 the gain b is indeed proportional to the speed of the actuator, estimated by applying a low-pass filter (LPF) to the derivative of the position x_{meas} measured by the encoder, Chiaradia et al. (2016).

Control performance has been evaluated by comparison between the FTF estimates in open (black line) and closed-loop (red line), in Fig. 2. The desired dynamic force is a chirp with amplitude 10 N and frequency linearly sweeping from 0.01 to 25 Hz. By looking at the open-loop FTF it is evident the significant notch-filter effects of the drop-off around the resonances, that is at 3 Hz, 7.5 Hz and with a more narrow-band fashion in the region between 13 and 15 Hz. Further disturbances provoke a noticeable attenuation of the measured force with respect to the reference since after 7 Hz, the mean value of the magnitude of the FTF stays about -18 dB. The phase diagram exhibits

shifts at frequencies that are consistent with the drop-offs of the magnitude plot. By looking at the closed-loop curve, we see that still, a distortion stands around 3 Hz. However, the magnitude decrease is more than halved compared to the open-loop curve. Whilst, above 7 Hz, the magnitude of the FTF is flat and about 0 dB, with negligible perturbations at the resonances, and all the phase shifts have been canceled out. We conclude that the control strategy mainly rejects the spectral distortions that affect the force transmissibility in the open-loop.

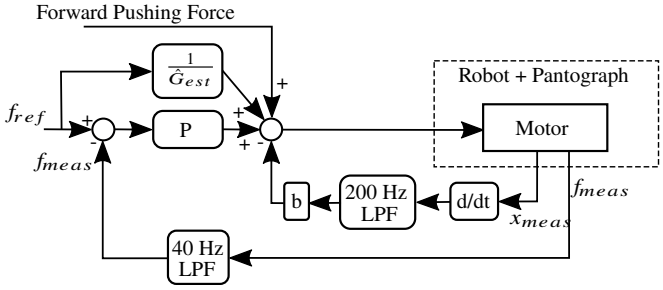

Fig. 3. Closed-feedback loop control scheme.

4. EXPERIMENTS DESCRIPTION

For this work, we have performed two kinds of experiments:

- a homogeneity test;
- a fault detection test.

The homogeneity test was meant to ascertain the nonlinear behavior of the pantograph in nominal conditions. To this goal, the receptance FRFs (see Eq. 1) were estimated and compared for two levels of the input force. Namely, force levels have been defined by the instantaneous amplitude of the relative chirp signal, which is 2 N (low level) and 11 N (high level). Furthermore, we focused on the interval 0 - 8 Hz because it combines sufficient dynamics information with the main nonlinear effects (due to dry friction). The high repeatability of the force-values that is guaranteed by the closed-loop enforces this choice, despite the residual distortion around 3 Hz.

On the other side, the fault detection capabilities of our device were investigated by simulating a localized fault. For each scenario, a homogeneity test was executed with the same aforementioned levels of force. As shown in Fig. 4, the pantograph frame is composed of two parallel planar mechanisms, which are connected through two diagonal bars. For this paper, we simulated the progressive loss of one of the bolt connections that joint one diagonal bar to the upper link of the frame, shown in 4 (a). Namely, 3 levels of intensity have been realized, that is: i) 50% of loss of preload; ii) 100% of loss of preload; iii) complete loss of the bolt, as in 4 (b). This kind of fault is interesting because it reproduces a real accident scenario, as described in Conway (2008). Also, it is particularly subtle, because, in each fault scenario, the global functionality of the frame is still ensured, because of the presence of the twin opposite bar.

The adopted sampling frequency is 1 kHz. In both kinds of tests, each FRF estimation was brought out repeating several times the forcing cycle, each with a duration of 120 s. Data records were windowed by the Hanning function, so as to attenuate the spectral distortions due to leakage. The FRF was computed through the Welch's averaged periodogram method. In particular, an H_1 estimator was adopted to attenuate noise on the output.

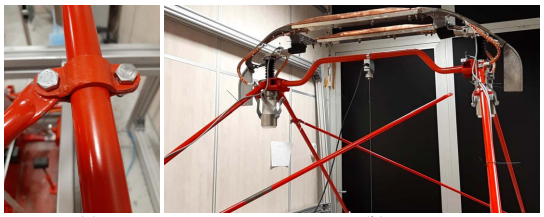

Fig. 4. (a) Detail of the bolted connection joining the diagonal bar to the pantograph frame. (b) Last level of the fault scenario, showing the complete loss of the bolt.

5. RESULTS AND DISCUSSION

5.1 Homogeneity test

Fig. 5 depicts the FRF (blue-solid line for low level, red-dotted line for high level) in the form of Bode plot.

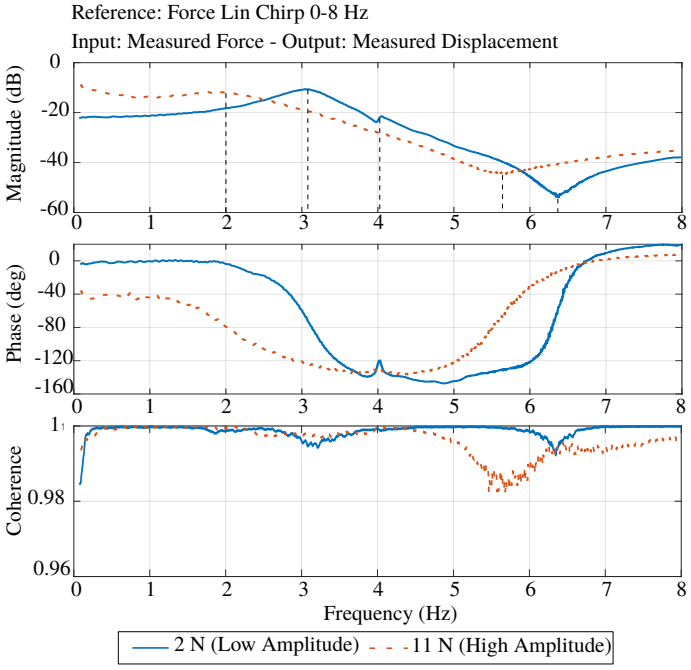

Fig. 5. Frequency Response Function estimates and input-output coherence for a safe pantograph for different levels on the input excitation.

In order to ascertain the quality of the FRF estimates, the input-output coherence function was estimated. The coherence γ^2 is a function of the frequency domain and represents the amount of output power that is linearly correlated with the input, as defined in:

$$\gamma^2(\omega) = 1 - \frac{S_{mm}(\omega)}{S_{xx}(\omega)} \tag{4}$$

where: S_{mm} and S_{xx} stand for the estimates of the auto-power spectral densities of the measurement noise m and output x respectively. From Eq. 4 it emerges that the coherence is 1 only if the noise power is zero. The lower diagram of Fig. 5 illustrates that except for some frequency regions, the coherence stays about 1, meaning a good input-output correlation.

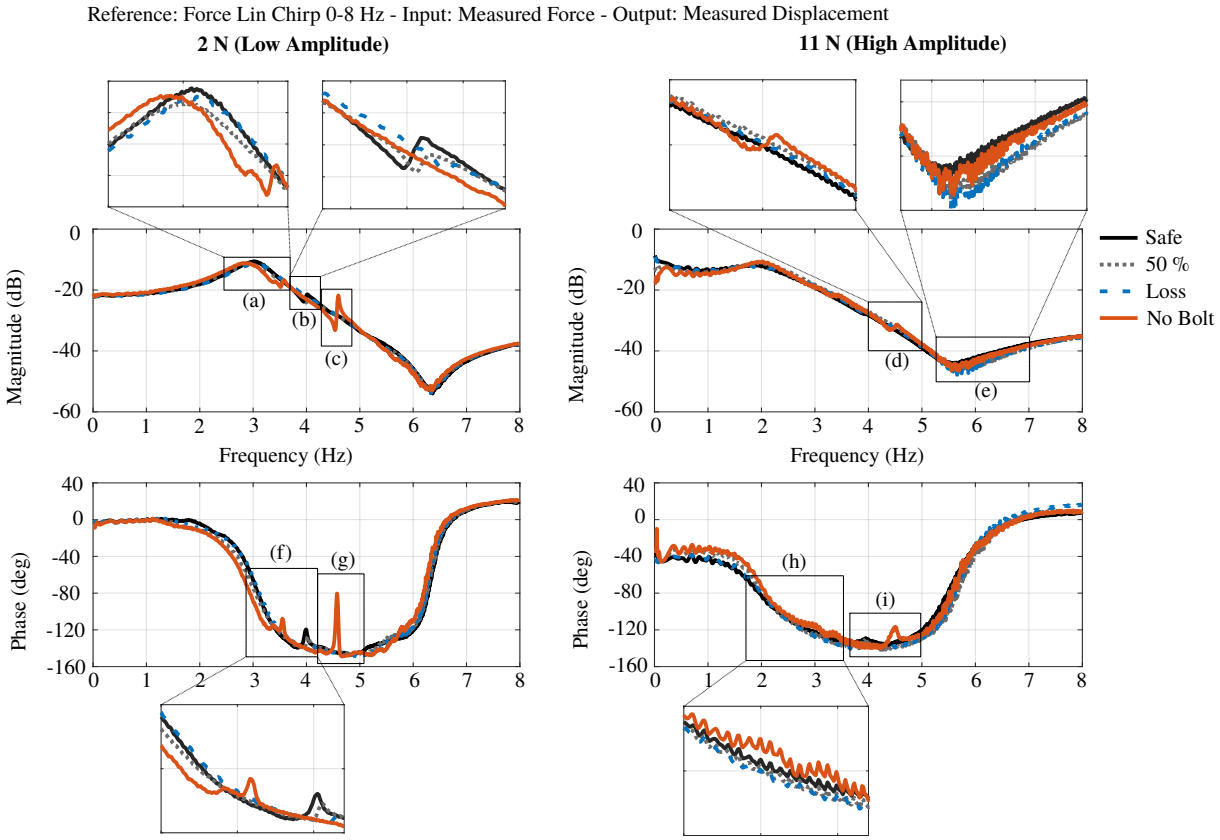

Fig. 6. Effect of a progressive loss in a bolt connection on the Frequency Response Function for low (left) and high level (right) of excitation. (a)-(i): enlargements showing the most sensitive distortions. In particular: black solid line: safe pantograph; gray, dotted line: 50% of loss of preload; blue dotted line: 100% of loss of preload; orange solid line: complete loss of the bolt.

From both the magnitude curves of Fig. 5, we clearly see the presence of one global maximum, associated with a first resonance, and a global minimum, associated with an anti-resonance, or *zero*. In particular, as the input level increases, the FRF results to be shifted towards the lower frequencies. In detail: i) the first peak stays almost constant in amplitude, while its frequency moves from 3 Hz to 2 Hz; ii) the zero exhibits an amplitude decrease, with a frequency shift from 6.2 Hz to 5.5 Hz. A further effect is the alteration of the FRF shape. It is evident the disappearance of a second resonance, present in the low-level FRF and highlighted by a little peak, at 4 Hz. Also, the sharpness of the first resonance peak is reduced, hinting stronger damping. To interpret this evidence, one should consider that: i) the pantograph response is determined by the coupling between the steel-frame mechanism and the elastic suspension; ii) damping is due to dry friction in the mechanism joints and to a viscous suspension damper. At low excitation level, some frame joints stay in a stick condition and hence the frame is isolated from the suspension damping. At high force level, static friction breaks out allowing the mechanical connection between the frame and the suspension which results in the severe damping of the second resonance.

5.2 Fault detection test

The Bode plots for the 3 fault scenarios are superimposed to the safe pantograph FRF in Fig. 6, for both low level (on the left) and high level of force (on the right). At low force level, the progressive loss of preload induces a slight modification: i) in the magnitude of the first resonance peak, Fig. 6 (a); ii) of the second resonance, about 4 Hz. Specifically, it can be observed that both the amplitude, Fig. 6 (b) and the phase shift, Fig. 6 (f) exhibit a progressive reduction with the increase of the damage level. In the remaining regions, FRFs are very close. Instead, the complete loss of the bolt provokes much more clear evidence. Indeed: i) two resonances appear at very close frequencies, at about 3.5 Hz, as highlighted by Fig. 6 (a) and Fig. 6 (f); ii) the second resonance of the safe system experiences a frequency shift, moving from 4 Hz to 4.5 Hz and assumes a magnified sharp shape of the magnitude, Fig. 6 (c) and exhibit a phase shift of about 60°, Fig. 6 (g).

At high force level, the progressive loss of preload gives only one clue, in the neighborhood of the zero, Fig. 6 (e), where it emerges a frequency shift and a progressive reduction of the amplitude, as long as a local separation of the curves with respect to the safe one. In addition, the relative difference between the two scenarios is much more contained with respect to the case of the low level of force. Instead, the loss of the bolt is still detectable by the alteration of the second resonance, Fig. 6 (d) and Fig. 6 (i). Furthermore, the two introduced resonances at about 3.5 Hz have disappeared from the magnitude plot, while survive with moderate phase shifts in Fig. 6 (h).

We can conclude that the progression of the loss of preload is hard to be identified because it alters locally the stiffness and the damping. In particular, the main damage hint happens at the second resonance, supposed to be related to a frame mode involving the bar. On the other side, the loss of the bolt changes the structural function of the bar, which behaves like a cantilever. Hence the two introduced new resonances are

related to the bending modes of the cantilever. Therefore it is advantageous to exploit the nonlinear characteristic of the system for damage detection since the detectability of faults itself is dependent on the input level. In particular, for all damage scenarios, detectability is enhanced by the low level of force. This is because the structural alterations provoked by the damage are sensitive to the damping phenomena that are triggered when joints switch from stick to slip condition, thus allowing the suspension damper to modify the dynamics of the system.

6. CONCLUSION

The introduction of robotics in the railway industry can significantly enhance maintenance efficiency. In this paper, we presented a robotic device meant to execute a periodic inspection of railway pantographs. In particular, the robot drives the structure into a dynamic test, by applying the desired force law and acquiring the consequent response and actual input force, thus reconstructing the Frequency Response Function. A first advance is that the robot is endowed with an innovative macro-micro actuation which is proved to increase the limited bandwidth achieved by actual devices. Furthermore, we discuss how the use of control is fundamental to delve deeper into the identification process. In detail, force control reveals to be necessary to ascertain the nonlinear characteristic of the pantograph. A direct hybrid control strategy is described and shown to sensibly contain the effect of disturbances. In the last part, we have simulated a minor localized damage that is the progressive loss in a bolt connection, from the partial reduction of preload up to the complete loss of the bolt. Results show that the preload attenuation is hard to be detected, though around certain frequencies FRF alterations emerge and could be correlated to the level of the damage. Instead, several clues hint the occurrence of the bolt loss. The main contribution is that for all the scenarios of this kind of fault, the effects of damage on the measured FRF are heightened for low excitation levels, due to nonlinear friction phenomena. Besides, it should be highlighted that both the architecture and method might be extended to the characterization of a general mechanical structure, especially when suspension and joints nonlinearity are suspected to arise. In future work, our approach will be to investigate a broader class of defects in a wider frequency range.

REFERENCES

Bing, C., S., X., Y., G., Q., Z., and J., D. (2018). Pantograph test method, system, device and rail vehicle. URL `https://bit.ly/2UN8k6K`. Patent ref.: CN106338405 (A).

Bruni, S., Facchinetti, A., Kolbe, M., Massat, J., et al. (2011). Hardware-in-the-loop testing of pantograph for homologation. In *9th World Congress on Railway Research WCRR*.

Chiaradia, D., Solazzi, M., Caporali, D., Russo, M., Piu, A., and Frisoli, A. (2016). Haptic simulation of an automotive automatic gearshift: Stability analysis and design of force profiles with hysteresis. In *2016 IEEE International Conference on Robotics and Automation (ICRA)*, 2663–2668. doi: 10.1109/ICRA.2016.7487426.

Conway, S. (2008). Review of human factors risk in rail vehicle maintenance and inspection. Technical report.

Deml, J., Baldauf, W., and Deutsche Bahn, A. (2001). A new test bench for examinations of the pantograph-catenary interaction. In *Proc. WCRR*, 25–29.

Ewins, D.J. (1984). *Modal testing: theory and practice*, volume 15. Research studies press Letchworth.

Fanning, P., Carden, E., and Terrace, E. (2003). A damage detection algorithm based on siso measurements. *ASCE Journal of Engineering Mechanics, 29 (2)*, 202–209.

Fanning, P.J. and Carden, E.P. (2004). Experimentally validated added mass identification algorithm based on frequency response functions. *Journal of Engineering Mechanics*, 130(9), 1045–1051.

Lu, G. (1998). Portable pantograph tester. URL `https://bit.ly/2IZLTcd`. Patent ref.: CN2316662 (Y).

McKelvey, T. and Guérin, G. (2012). Non-parametric frequency response estimation using a local rational model. In *IFAC Proceedings. 16th IFAC Symposium on System Identification*, volume 16, 49–54.

Morrell, J.B. and Salisbury, J.K. (1998). Parallel-coupled micro-macro actuators. *The International Journal of Robotics Research*, 17(7), 773–791.

Peters, J. (1981). Dead line testing of pantographs on the rtt catenary system. Technical report.

Peterson, E.L. (1993). Modal excitation: Good data not bad data. In *Proceedings-SPIE The International Society for Optical Engineering*, 1161–1161. SPIE The International Society for Optical.

R.A.I.B. (2013). Report 06/2013: Accident involving a pantograph and the overhead line near Littleport. Technical report.

Santamato, G., Chiaradia, D., Solazzi, M., and Frisoli, A. (2019). A lightweight robotic device for the inspection of railway pantograph. In *2019 IEEE International Symposium on Safety, Security, and Rescue Robotics (SSRR)*, 284–289. IEEE.

Santamato, G., Marcheschi, S., Solazzi, M., and Frisoli, A. (2018). A hybrid actuation system for a portable structural health monitoring device. In *The International Conference of IFToMM ITALY*, 397–405. Springer.

Sohn, H., Farrar, C.R., Hemez, F.M., Shunk, D.D., Stinemates, D.W., Nadler, B.R., and Czarnecki, J.J. (2003). A review of structural health monitoring literature: 1996–2001. *Los Alamos National Laboratory, USA*.

Stern, S. (2017). The rail sector' s changing maintenance game. Technical report.

Worden, K. (2019). *Nonlinearity in structural dynamics: detection, identification and modelling*. CRC Press.

Worden, K., Farrar, C.R., Haywood, J., and Todd, M. (2008). A review of nonlinear dynamics applications to structural health monitoring. *Structural Control and Health Monitoring: The Official Journal of the International Association for Structural Control and Monitoring and of the European Association for the Control of Structures*, 15(4), 540–567.

Xie, C., Long, Z., Peng, X., and Z., X. (2009). Detection method and system device for characteristics of locomotive pantograph. URL `https://bit.ly/2VENZoN`. Patent ref.: CN104897423 (A).

Xin, T., Roberts, C., Weston, P., and Stewart, E. (2018). Condition monitoring of railway pantographs to achieve fault detection and fault diagnosis. *Proceedings of the Institution of Mechanical Engineers, Part F: Journal of Rail and Rapid Transit*, 0954409718800567.

Zhang, W., Zou, D., Tan, M., Zhou, N., Li, R., and Mei, G. (2018). Review of pantograph and catenary interaction. *Frontiers of Mechanical Engineering*, 13(2), 311–322.